Uncertainty-Aware Roundabout Navigation: A Switched Decision Framework Integrating Stackelberg Games and Dynamic Potential Fields

Zhihao Lin[1†], Zhen Tian[1†], Jianglin Lan[1], Dezong Zhao[1§], *Senior Member, IEEE*, and Chongfeng Wei[1], *Senior Member, IEEE*

***Abstract*—Roundabout navigation presents significant challenges for autonomous vehicles (AVs) due to complex multi-vehicle interactions, highly dynamic and uncertain traffic patterns, and the requirement to coordinate with multiple vehicles simultaneously. Existing approaches often struggle to maintain safety and efficiency in uncertain vehicle behaviors and space-constrained situations, especially for mandatory lane changes and exit maneuvers. This paper presents a switched decision system that combines game theory and potential fields to enable robust navigation in roundabouts. The proposed approach first develops a Stackelberg game framework with uncertainty-aware prediction, where AVs dynamically adjust their decisions based on probabilistic estimates of surrounding vehicles' behaviors. Additionally, a hybrid potential field method is introduced that seamlessly transitions to emergency maneuvering when standard game-theoretic solutions become infeasible. Through extensive simulations under varied scenarios, the proposed approach achieves 97% successful navigation rates while maintaining collision rates below 1%, significantly outperforming baseline Nash equilibrium methods. The results demonstrate that integrating uncertainty characterization with strategic cooperation significantly improves the overall safety and efficiency of autonomous driving in roundabouts.**

***Index Terms*—Autonomous vehicles, uncertainty-aware prediction, Stackelberg game theory, hybrid potential fields.**

I. INTRODUCTION

INTELLIGENT vehicles have become increasingly common in daily life, with autonomous vehicles (AVs) expected to reach 54 million globally by 2025 [1]. AVs can effectively mitigate safety incidents resulting from human errors such as fatigue, distraction, and delayed response [2], [3]. Furthermore, AVs can compute optimal decision-making solutions more rapidly than human drivers, thus enhancing traffic efficiency [4], [5]. Roundabouts are widely used in various traffic scenarios due to their higher capacity and fewer conflict points [6]. Recent designs for many roundabouts cater to the needs of AVs and connected autonomous vehicles (CAVs), optimizing traffic flow and safety [7]–[9].

Despite these advantages, autonomous navigation in roundabouts presents unique challenges that remain inadequately addressed [10]. The circular geometry, continuous traffic flow, and complex vehicle interactions create an environment where decisions must be made within limited spatial and temporal windows [11]. Current approaches often fail to adequately address three critical aspects: uncertainty in trajectory prediction, balancing cooperative and competitive behaviors, and ensuring safety during emergency maneuvers [12], [13]. These challenges are particularly pronounced when AVs interact with human-driven vehicles (HDVs), as their decision-making patterns differ significantly—AVs follow programmed rules while HDVs rely on intuition, experience, and social cues [14], [15]. The interplay between these three challenges creates a cascading effect in roundabout navigation. Uncertainty in trajectory prediction undermines both cooperative planning and emergency response capabilities. When prediction confidence degrades—particularly in curved geometries where sensor occlusions and dynamic interactions are prevalent—game-theoretic approaches struggle to compute reliable equilibria due to expanded strategy spaces and increased computational complexity. This computational burden becomes prohibitive in time-critical scenarios, necessitating a fundamentally different approach. Thus, our framework addresses these challenges through a hierarchical architecture: uncertainty-aware prediction forms the foundation, game-theoretic planning operates under normal conditions with manageable uncertainty, and potential field methods provide fail-safe emergency response when either uncertainty exceeds thresholds or computational constraints prevent strategic planning.

Existing decision-making frameworks for autonomous driving in roundabouts can be broadly categorized into three approaches: game-theoretic methods, reinforcement learning techniques, and potential field-based systems [16]. Each approach offers distinct advantages but also exhibits specific limitations when applied to roundabout navigation [17].

Game-theoretic approaches model the strategic interactions between vehicles, enabling AVs to make decisions while anticipating other vehicles' responses [18]. For instance, [19] proposes a Stackelberg game model for lane-changing, while [20] and [21] emphasize balancing safety, efficiency, and comfort through Nash equilibrium concepts. However, these methods often lead to overly conservative behaviors in practical implementations [22], [23] and struggle with computational efficiency in time-critical scenarios [24], [25]. Their fundamental limitation in emergency situations is twofold: the computational complexity of solving for equilibria causes delayed responses, while their focus on strategic optimization

This work was supported in part by the China Scholarship Council Ph.D. Scholarship for 2023-2027 (No.202206170011).

[1]Zhihao Lin, Zhen Tian, Jianglin Lan, Dezong Zhao, and Chongfeng Wei are with the James Watt School of Engineering, University of Glasgow, Glasgow G12 8QQ, United Kingdom.

§Corresponding author. Dezong Zhao(e-mail: dezong.zhao@glasgow.ac.uk)

† Equal contribution

may not adequately prioritize immediate safety when space is constrained.

Reinforcement learning (RL) approaches have shown promise for complex traffic scenarios [26], [27]. Recent work [28] applies deep Q-networks to model lane-changing decisions in roundabouts, learning optimal policies through environmental interactions. [29] employs proximal policy optimization for multi-agent roundabout navigation, while [30] extends soft actor-critic methods with safety constraints through barrier functions [31]. Despite these advances, RL-based approaches face significant challenges: they require extensive training data that rarely covers all edge cases, lack explainability in their learned policies, and struggle to provide formal safety guarantees [32]. The "reality gap" between simulation and real-world deployment remains substantial [33], particularly in dynamic and uncertain roundabout environments.

Potential field methods offer a reactive approach to navigation, applying concepts of attractive and repulsive forces to guide vehicles [34]. [35] applies improved artificial potential fields to traffic scenarios, [36] incorporated dynamic risk assessment based on time-to-collision metrics. [37] proposed velocity-dependent potential fields that adjust force magnitudes based on relative speeds [38]. However, conventional implementations suffer from local minima problems in complex roundabout geometries [39]. Some hybrid approaches have shown integrated potential fields with Model Predictive Control (MPC), [40] combined potential fields with fuzzy logic [41]. Despite these improvements, existing potential field applications typically lack strategic planning capabilities and fail to account for growing uncertainties in vehicle state prediction within curved geometries [42].

Our analysis reveals challenges in autonomous roundabout navigation: insufficient uncertainty characterization in curved trajectories, poor balance between cooperative and competitive behaviors, and inadequate solutions for emergency scenarios [43]. To address these challenges, we present a switched decision system integrating Stackelberg game theory with hybrid potential fields. Our approach employs time-varying uncertainty models and non-selfish utility functions for normal driving, while dynamically transitioning to emergency mode when computational or spatial constraints demand it. The key contributions are as follows:

- The proposed work presents an uncertainty-aware switched decision system for roundabout navigation, integrating probabilistic prediction with game theory and potential fields for robust decision-making.
- A Stackelberg game framework is developed incorporating time-varying uncertainty bounds in the prediction of surrounding vehicles' behaviors. This approach provides adaptive decision-making capabilities for normal driving conditions through uncertainty-aware strategic planning.
- A hybrid potential field method is introduced with quintic polynomial trajectories for emergency scenarios when game-theoretic solutions become computationally intractable or spatially infeasible. This complementary approach ensures safety and efficiency during critical maneuvers like urgent lane changes.

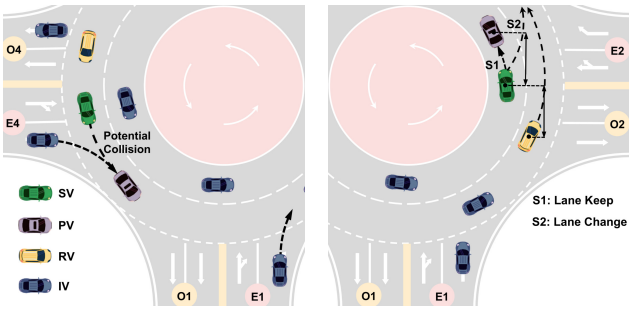

(a) (b)

Fig. 1: Several challenging scenarios: (a) potential collision (b) the emergencies lane-changing process with two possible strategies: S1 and S2.

The rest of this paper is organized as follows. Section II describes the problem statement and system structure. Section III describes the decision process with game theory. Section IV introduces the vehicle prediction and control model. Section V describes the decision model with the hybrid field. Section VI presents simulation results and comparative analysis. Section VII draws the conclusions.

II. Problem Statement and System Structure

1) Problem Formulation Consider a roundabout environment as shown in Fig. 1, where the autonomous vehicle (denoted as SV) interacts with three types of surrounding vehicles: proceeding vehicle (PV), rear vehicle (RV), and interactive vehicles (IV), referring to other nearby vehicles that may influence the SV's behavior through implicit interaction. Let $\mathcal{V} = \{\text{SV}, \text{PV}, \text{RV}, \text{IV}\}$ denote the set of vehicles. Each vehicle $i \in \mathcal{V}$ has a state vector $\mathbf{x}_i = [x_i, y_i, \phi_i, v_i]^\top$, where (x_i, y_i) represents position, ϕ_i denotes heading angle, and v_i is velocity.

The roundabout geometry imposes specific spatial constraints on vehicle navigation:

$$\begin{aligned} \mathcal{X}_{\text{road}}: &\quad r_{\text{inner}} \le \|\mathbf{p}_{\text{SV}} - \mathbf{c}\| \le r_{\text{outer}}, \\ \mathcal{X}_{\text{safe}}: &\quad \|\mathbf{p}_{\text{SV}} - \mathbf{p}_j\| \ge d_{\text{safe}}, \quad \forall j \in \{\text{PV}, \text{RV}, \text{IV}\}, \end{aligned} \tag{1}$$

where r_{inner} and r_{outer} define the roundabout boundaries, $\mathbf{c}$ is the center, $\mathbf{p}$ denotes the 2D position vector of each vehicle, and d_{safe} is the minimum safety distance.

Within these constraints, the decision-making problem for the SV is formulated as:

$$\begin{aligned} \min_{\mathbf{u}_{\text{SV}}} \quad & J(\mathbf{x}_{\text{SV}}, \mathbf{u}_{\text{SV}}, \mathbf{X}_{\text{env}}) \quad \text{s.t.} \quad \dot{\mathbf{x}}_{\text{SV}} = f(\mathbf{x}_{\text{SV}}, \mathbf{u}_{\text{SV}}), \\ & \mathbf{x}_{\text{SV}} \in \mathcal{X}_{\text{road}} \cap \mathcal{X}_{\text{safe}}(\mathbf{X}_{\text{env}}), \ \mathbf{u}_{\text{SV}} \in \mathcal{U}, \end{aligned} \tag{2}$$

where $\mathbf{u}_{\text{SV}}$ represents control inputs (acceleration, steering), $\mathbf{X}_{\text{env}} = [\mathbf{x}_{\text{PV}}^\top, \mathbf{x}_{\text{RV}}^\top, \mathbf{x}_{\text{IV}}^\top]^\top$ denotes environment state, and $\mathcal{U}$ represents the admissible control set. The constraints ensure the vehicle remains within the roundabout boundaries while maintaining safe distances from other vehicles.

The objective function J incorporates safety, efficiency, and comfort:

$$J = w_s J_{\text{safety}} + w_e J_{\text{efficiency}} + w_c J_{\text{comfort}}, \tag{3}$$

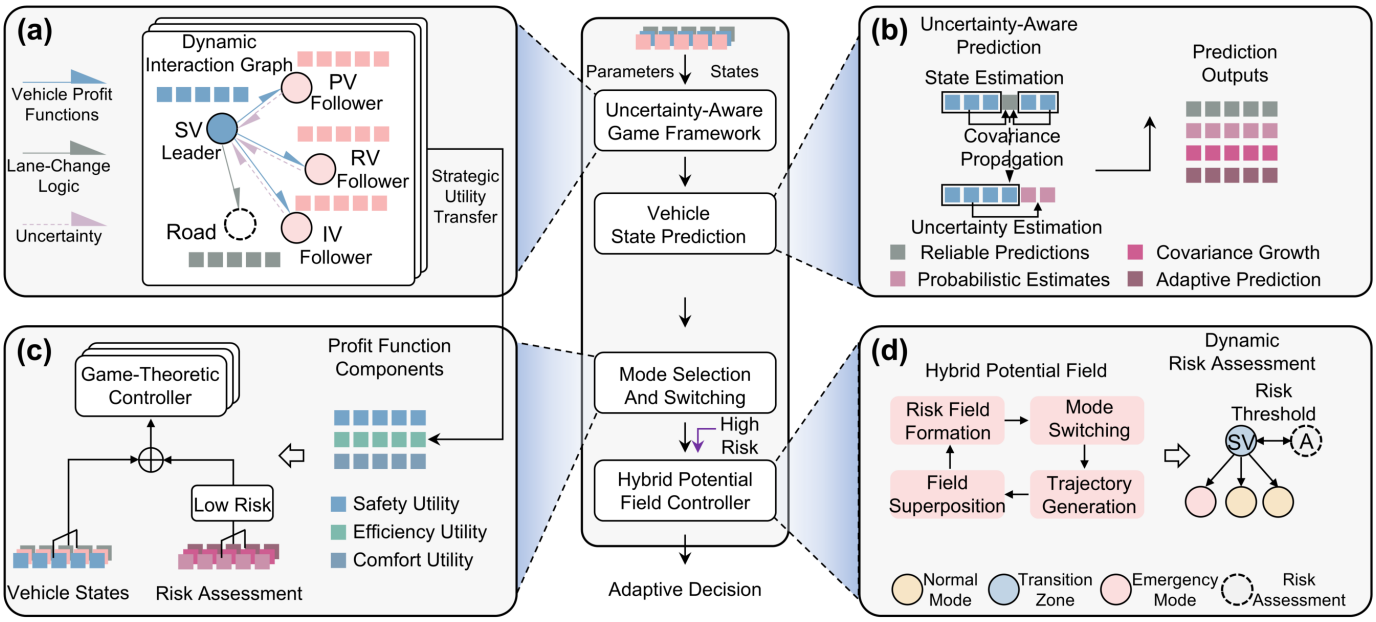

Fig. 2: System architecture of the uncertainty-aware switched decision framework for roundabout navigation.

where w_s, w_e, and w_c are corresponding weights. This objective function provides a unified structure for balancing safety, efficiency, and comfort. The weights are prioritized as $w_s > w_e > w_c$, with values $w_s = 0.6$, $w_e = 0.3$, and $w_c = 0.1$ selected via simulation to reflect roundabout-specific trade-offs. This formulation is later instantiated in the Stackelberg model (Section III) and the uncertainty-aware predictor (Section IV).

2) Emergency Scenario Characterization An emergency scenario is defined through a composite risk assessment:

$$\mathcal{E}(t) = \begin{cases} \text{Emergency}, & \text{if } \Gamma(t) \geq \Gamma_{\text{thr}}(t) \\ \text{Normal}, & \text{otherwise} \end{cases}, \tag{4}$$

where $\Gamma(t)$ is a continuous risk function aggregating computational feasibility $\tau_{\text{comp}}(t)/\tau_{\max}$ ($\tau_{\max} = 100$ ms), spatial constraint ratio $S(t) = d_{\text{avail}}(t)/d_{\text{req}}(t)$ (critical at 1.2), and prediction uncertainty $\mathcal{U}_{\text{pred}}(t) = \text{tr}(\mathbf{\Sigma}(t))/\text{tr}(\mathbf{\Sigma}0)$ (threshold 3). The emergency mode is triggered when $\Gamma(t)$ exceeds the adaptive threshold $\Gamma\text{thr}(t)$, enabling smooth transitions between operational modes via continuous risk assessment rather than discrete switching.

3) System Structure Our framework, illustrated in Fig. 2, integrates three functional layers working in tandem. The prediction layer implements uncertainty-aware state estimation through covariance matrices $\mathbf{\Sigma}_j(t)$ and adaptive horizon adjustment via confidence measure $\alpha_j(i)$. The decision layer employs a dual-mode strategy that dynamically switches between approaches based on risk assessment. During normal operation, a Stackelberg game-theoretic approach optimizes interactions by balancing safety, efficiency, and comfort objectives, with the AV (as leader) anticipating followers' responses. However, this approach becomes computationally prohibitive in emergency scenarios. For these situations, the system transitions to a hybrid potential field method combining dynamic risk assessment $R_i(x, y)$ with polynomial trajectories. This switching mechanism leverages complementary strengths—strategic planning from game theory and reactive capability from potential fields. The control layer executes these decisions using MPC [44], accounting for model uncertainties and the roundabout's curved geometry.

III. Game Theory Approach for Cooperative Roundabout Navigation

Our adaptive game-theoretic approach is presented to promote cooperation between autonomous and human-driven vehicles in roundabouts. We first establish a unified profit function framework, then customize it for specific vehicle types, and finally formulate the Stackelberg equilibrium solution that governs optimal control strategies.

A. General Profit Function Framework

To model vehicle interactions in the roundabout scenario, we establish a unified profit function framework applicable to all vehicles, with appropriate adaptations for each vehicle type. For any vehicle $i \in \{\text{SV}, \text{RV}, \text{PV}, \text{IV}\}$, the general profit function is constructed as:

$$P_i = C_{\text{s}}^i U_{\text{s}}^i + C_{\text{e}}^i U_{\text{e}}^i + C_{\text{c}}^i U_{\text{c}}^i, \tag{5}$$

where C_{s}^i, C_{e}^i, and C_{c}^i are coefficients for safety, efficiency, and comfort respectively, and U_{s}^i, U_{e}^i, and U_{c}^i represent the corresponding utility components.

B. Safety Utility

The safety utility for vehicle i with respect to surrounding vehicles is defined as:

$$U_{\text{s}}^i = \sum_{j \in \mathcal{N}_i} k_{\text{s}}^{i-j} U_{\text{S}}^{i-j}, \tag{6}$$

where $\mathcal{N}_i$ represents the set of neighboring vehicles that i interacts with, k_{s}^{i-j} is the safety coefficient between vehicles i and j, and U_{S}^{i-j} represents the safety utility for their interaction. For any vehicle pair (i, j), this interaction safety utility is defined using a distance-based threshold function:

$$U_{\text{S}}^{i-j} = \begin{cases} 0 & \text{if } d_{i-j} > \epsilon_i^j d_{\text{safe}} \\ f_i(d_{i-j}, \epsilon_i^j, d_{\text{safe}}) & \text{otherwise} \end{cases}, \tag{7}$$

where ϵ_i^j is an attention allocation coefficient from vehicle i to vehicle j, d_{i-j} is the distance between them, and d_{safe} is the minimum safe distance. The function f_i differs between autonomous and human-driven vehicles:

$$f_i(d, \epsilon, d_{\text{safe}}) = \begin{cases} \frac{1}{\epsilon \cdot d_{\text{safe}}} - 1 & \text{if } i \text{ is human-driven} \\ 1 - \frac{1}{\epsilon \cdot d_{\text{safe}}} & \text{if } i \text{ is autonomous} \end{cases} \tag{8}$$

reflecting their different safety response characteristics.

C. Efficiency Utility

The efficiency utility for vehicle i is defined as:

$$U_{\text{e}}^i = \sum_{j \in \mathcal{N}_i} k_{\text{e}}^{i-j} U_{\text{EFFI}}^{i-j} + k_{\text{e}}^{i-\text{NR}} U_{\text{NORMAL}}^{i-\text{NR}}, \tag{9}$$

where k_{e}^{i-j} and $k_{\text{e}}^{i-\text{NR}}$ are efficiency coefficients for interactions with neighboring vehicles and normal driving speed, respectively. For any vehicle pair, the relative efficiency utility is:

$$U_{\text{EFFI}}^{i-j} = \frac{V_i}{V_i + V_j}, \quad U_{\text{NORMAL}}^{i-\text{NR}} = \frac{V_i}{V_i + V_{\text{NR}}}, \tag{10}$$

where V_i, V_j, and V_{NR} represent the current speed of vehicle i, vehicle j, and the normal driving speed, respectively.

D. Comfort Utility

The comfort utility for any vehicle is defined as:

$$U_{\text{c}}^i = \left(\frac{a_i}{a_{\max}}\right)^2, \tag{11}$$

where a_i is the vehicle's acceleration and $a_{\max}$ is the maximum acceleration.

E. Vehicle Adaptation and Lane-Change Logic

Each vehicle type adapts the general profit function framework to its role. The autonomous SV prioritizes safety over efficiency and comfort with the weighting structure ($C_{\text{s}}^{\text{SV}} > C_{\text{e}}^{\text{SV}} > C_{\text{c}}^{\text{SV}}$). We adopt the Stackelberg framework as a modeling approximation. While real-world driving involves simultaneous decision-making, the leader-follower structure captures the proactive nature of autonomous vehicles that can commit to actions more consistently than human drivers.

To determine lane-changing timing, SV evaluates a lane-change-specific profit function $P_{\text{SV}}^{\text{LC}}(nT)$ at each game step n. A lane change is triggered at time $T_{\text{LC}} = nT$ if the accumulated utility exceeds a threshold:

$$T_{\text{LC}} = nT \quad \text{if } P_{\text{SV}}^{\text{LC}}(nT) \geq \tau_{\text{LC}}, \tag{12}$$

where τ_{LC} reflects the minimum utility required to justify a safe and efficient lane change. Superscript LC indicates that the profit function is specific to lane-changing. The profit function is then defined as:

$$P_{\text{SV}}^{\text{LC}}(nT) = \frac{d_{\text{SV-RV}} \left\| U_{\text{S}}^{\text{SV-RV}} N_{\text{s}} + \gamma n \right\|_2^2}{P_{\text{RV}}}, \tag{13}$$

where $d_{\text{SV-RV}}$ is the distance between SV and the RV, $U_{\text{S}}^{\text{SV-RV}}$ is the pairwise safety utility, N_{s} denotes the duration of stable interaction, and γ is a time discount factor. This formulation encourages lane changes only after sufficient stability and favors earlier transitions when safety conditions are met.

F. Stackelberg Equilibrium

We integrate the profit functions of SV, RV, IV, and PV in (5) into a unified Stackelberg game-theoretic framework that formalizes each vehicle's objectives and lane-changing decisions. Building on this foundation, we formulate a hierarchical optimization problem where the SV acts as the leader and strategically anticipates the responses of surrounding HDV (followers). This max-min structure provides robustness against worst-case rational responses within the followers' strategy spaces. The Stackelberg model captures the asymmetric nature of AV–HDV interactions and enables computation of equilibrium strategies that govern the SV's optimal control actions. The equilibrium solution is obtained through

$$\begin{aligned} \tilde{\mathbf{u}}_{\text{SV}}^* &:= \arg \max_{\tilde{\mathbf{u}}_{\text{SV}} \in \mathcal{U}_{\text{SV}}} \min_{\tilde{\mathbf{y}} \in \mathcal{Y}} P_{\text{SV}}(\tilde{\mathbf{u}}_{\text{SV}}, \tilde{\mathbf{y}}) \\ \mathbf{s.t.} \quad & \mathcal{Y} \triangleq \{\tilde{\mathbf{u}}_{\text{PV}} \in \mathcal{U}_{\text{PV}}^*, \tilde{\mathbf{u}}_{\text{RV}} \in \mathcal{U}_{\text{RV}}^*, \tilde{\mathbf{u}}_{\text{IV}} \in \mathcal{U}_{\text{IV}}^*\}, \end{aligned} \tag{14}$$

where the best-response strategy sets for each follower vehicle are defined as:

$$\begin{aligned} \mathcal{U}_{\text{PV}}^* \triangleq \{&\tilde{\mathbf{u}}_{\text{PV}} \in \mathcal{U}_{\text{PV}} : P_{\text{PV}}(\tilde{\mathbf{u}}_{\text{SV}}, \tilde{\mathbf{u}}_{\text{PV}}^*) \\ &\geq P_{\text{PV}}(\tilde{\mathbf{u}}_{\text{SV}}, \tilde{\mathbf{u}}_{\text{PV}}) \, \forall \tilde{\mathbf{u}}_{\text{PV}} \in \mathcal{U}_{\text{PV}}\}, \\ \mathcal{U}_{\text{RV}}^* \triangleq \{&\tilde{\mathbf{u}}_{\text{RV}} \in \mathcal{U}_{\text{RV}} : P_{\text{RV}}(\tilde{\mathbf{u}}_{\text{SV}}, \tilde{\mathbf{u}}_{\text{RV}}^*) \\ &\geq P_{\text{RV}}(\tilde{\mathbf{u}}_{\text{SV}}, \tilde{\mathbf{u}}_{\text{RV}}) \, \forall \tilde{\mathbf{u}}_{\text{RV}} \in \mathcal{U}_{\text{RV}}\}, \\ \mathcal{U}_{\text{IV}}^* \triangleq \{&\tilde{\mathbf{u}}_{\text{IV}} \in \mathcal{U}_{\text{IV}} : P_{\text{IV}}(\tilde{\mathbf{u}}_{\text{SV}}, \tilde{\mathbf{u}}_{\text{IV}}^*) \\ &\geq P_{\text{IV}}(\tilde{\mathbf{u}}_{\text{SV}}, \tilde{\mathbf{u}}_{\text{IV}}) \, \forall \tilde{\mathbf{u}}_{\text{IV}} \in \mathcal{U}_{\text{IV}}\}, \end{aligned} \tag{15}$$

where $\tilde{\mathbf{u}}_{\text{SV}}^*$ denotes the optimal control strategy, and $\tilde{\mathbf{y}} = [\tilde{\mathbf{u}}_{\text{PV}}^\top, \tilde{\mathbf{u}}_{\text{RV}}^\top, \tilde{\mathbf{u}}_{\text{IV}}^\top]^\top$ represents the environment state vector comprising follower vehicles' control strategies. The profit functions $P_i(\cdot)$ for each vehicle $i \in \{\text{SV}, \text{PV}, \text{RV}, \text{IV}\}$ are defined based on the utility components in (5) and evaluate the rewards for chosen control strategies.

This Stackelberg formulation embeds the unified profit functions into a sequential decision framework that models strategic interactions among vehicles. Solving for its equilibrium yields control strategies that account for both individual objectives and predicted responses of others, encouraging cooperative behavior crucial for safe roundabout navigation. These decisions form the basis of a MPC execution layer, where follower strategies are encoded in an abstract environment state vector $\tilde{\mathbf{y}}$ and physical states $\mathbf{y}$ are used for trajectory planning. Accurate prediction of surrounding vehicles is essential to ensure robust execution, which is addressed next via a stochastic modeling approach.

IV. Vehicle Kinematics and Uncertainty-Aware State Prediction

This section introduces a stochastic vehicle prediction framework for risk-aware decision-making in roundabouts. A nonlinear vehicle model with uncertainty propagation is constructed and linearized to enable adaptive prediction of surrounding vehicles' behaviors under dynamic conditions.

A. Vehicle Kinematics and Constraints

The motion of vehicles in the roundabout is described by a stochastic kinematic bicycle model with nonholonomic constraints:

$$\begin{bmatrix}\dot{x} & \dot{y} & \dot{\phi}\end{bmatrix}^\top = v \cdot \begin{bmatrix}\cos(\phi) & \sin(\phi) & \frac{\tan(\delta)}{L}\end{bmatrix}^\top + \mathbf{w}(t), \quad (16)$$

where $\mathbf{w}(t) \sim \mathcal{N}(0, \mathbf{Q}(t))$ captures modeling errors and external disturbances, (x, y) represents the vehicle's position, ϕ is the heading angle, v is the velocity, L is the wheelbase, and δ is the steering angle. Here, $\mathbf{Q}(t)$ is the process noise covariance matrix, characterizing the intensity and correlation structure of the stochastic disturbances. In addition, let $\hat{\mathbf{x}}(t)$ be an estimate of the true state $\mathbf{x}(t)$. The state estimation error $\mathbf{e}(t) = \mathbf{x}(t) - \hat{\mathbf{x}}(t)$ is defined, and its associated covariance matrix is expressed as

$$\mathbf{P}(t) = \mathbb{E}\big[\mathbf{e}(t)\mathbf{e}^\top(t)\big]. \quad (17)$$

This matrix $\mathbf{P}(t)$ quantifies our uncertainty about the state estimate. As will be shown later, $\mathbf{P}(t)$ evolves according to a Lyapunov-type differential equation influenced by $\mathbf{Q}(t)$.

The system operates under physical constraints:

$$|v| \le v_{\max}, \quad |\delta| \le \delta_{\max}, \quad |a| \le a_{\max}, \quad (18)$$

where $v_{\max}$ represents the maximum allowable velocity magnitude, $\delta_{\max}$ represents the maximum steering angle (typically mechanically limited), and $a_{\max}$ represents the maximum acceleration/deceleration magnitude.

For controller design and stability analysis, we express the nonlinear system in a compact form:

$$\dot{\mathbf{x}} = f(\mathbf{x}, \mathbf{u}, \mathbf{y}) + \mathbf{w}(t) \quad (19)$$

with state vector $\mathbf{x} = [x, y, \phi]^\top$, control input $\mathbf{u} = [v, \delta]^\top$, and environment state vector $\mathbf{y} = [\mathbf{x}_{\text{PV}}^\top, \mathbf{x}_{\text{RV}}^\top, \mathbf{x}_{\text{IV}}^\top]^\top$ representing surrounding vehicles' states.

To enable efficient computation in MPC, we linearize the system around a reference trajectory $\mathbf{x}_r$ through first-order Taylor expansion:

$$\dot{\mathbf{x}} = f(\mathbf{x}_r, \mathbf{u}_r, \mathbf{y}_r) + J_1(\mathbf{x} - \mathbf{x}_r) + J_2(\mathbf{u} - \mathbf{u}_r) + J_3(\mathbf{y} - \mathbf{y}_r), \quad (20)$$

where J_1, J_2, and J_3 are the Jacobian matrices with respect to the state vector, control input, and environment state, respectively. By defining the error states $\tilde{\mathbf{x}} = \mathbf{x} - \mathbf{x}_r$, $\tilde{\mathbf{u}} = \mathbf{u} - \mathbf{u}_r$, and $\tilde{\mathbf{y}} = \mathbf{y} - \mathbf{y}_r$, we obtain the linearized error dynamics:

$$\dot{\tilde{\mathbf{x}}} = J_1\tilde{\mathbf{x}} + J_2\tilde{\mathbf{u}} + J_3\tilde{\mathbf{y}} + \mathbf{w}(t). \quad (21)$$

This formulation supports state prediction and control design while accounting for interactions with surrounding vehicles. Detailed Jacobian matrix derivations and linearization are provided in Appendix A.

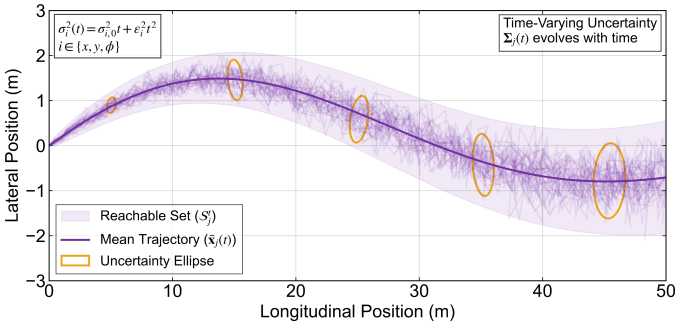

Fig. 3: Trajectory prediction visualization showing: mean trajectory $\bar{\mathbf{x}}_j(t)$ (purple line), uncertainty ellipsoids derived from $\mathbf{\Sigma}_j(t)$ (orange ellipses), and the probabilistic reachable set $\mathcal{S}_j^t$ (shaded region). The uncertainty grows according to $\sigma_i^2(t) = \sigma_{i,0}^2 t + \epsilon_i^2 t^2$ for $i \in \{x, y, \phi\}$.

B. Adaptive Prediction with Time-Varying Uncertainty

Robust prediction in roundabouts requires modeling how sensing and behavioral uncertainties evolve over time. Based on the stochastic vehicle model in (19), we formulate an adaptive prediction framework that captures both deterministic motion and the temporal growth of uncertainty in vehicle states.

For surrounding vehicle $j \in \{\text{PV}, \text{RV}, \text{IV}\}$, the state evolution follows:

$$\dot{\mathbf{x}}_j(t) = f(\mathbf{x}_j(t), \mathbf{u}_j(t), \mathbf{y}_j(t)) + \mathbf{w}_j(t), \quad (22)$$

where $\mathbf{w}_j(t)$ represents the process uncertainty. The predicted trajectory over horizon $[t_0, t_0 + T]$ is characterized by:

$$\mathbf{x}_j(t) = \int_{t_0}^{t} f(\mathbf{x}_j(\tau), \mathbf{u}_j(\tau), \mathbf{y}_j(\tau))\mathrm{d}\tau + \boldsymbol{\epsilon}_j(t), \quad (23)$$

with $\boldsymbol{\epsilon}_j(t) \sim \mathcal{N}(0, \mathbf{\Sigma}_j(t))$ capturing the accumulated prediction uncertainty.

The uncertainty propagation follows a time-varying covariance structure:

$$\mathbf{\Sigma}_j(t) = \mathrm{diag}\big(\sigma_x^2(t), \sigma_y^2(t), \sigma_\phi^2(t)\big), \quad (24)$$

where the diagonal elements evolve according to:

$$\sigma_i^2(t) = \sigma_{i,0}^2 t + \epsilon_i^2 t^2, \quad i \in \{x, y, \phi\}, \quad (25)$$

where $\sigma_{i,0}^2$ represents the initial variance for each state component, and ϵ_i^2 denotes the growth rate parameter that captures how uncertainty increases over time for the position coordinates (x, y) and heading angle ϕ.

To account for the evolution of prediction uncertainty in a systematic manner, we first defined the time-varying covariance structure $\mathbf{\Sigma}_j(t)$ in (24). However, this formulation primarily captures deterministic growth patterns of uncertainty under idealized assumptions.

For a more rigorous characterization, especially when considering the linearized error dynamics in (21), the state estimation error covariance $\mathbf{P}$ evolves over time according to the Lyapunov-type differential equation:

$$\dot{\mathbf{P}} = J_1\mathbf{P} + \mathbf{P}J_1^\top + \mathbf{Q}(t), \quad (26)$$

where $\mathbf{P}$ reflects the propagation of stochastic uncertainties in the state estimation. (26) complements the earlier definition of $\mathbf{\Sigma}_j(t)$ by accounting for the linearized system dynamics and process noise covariance $\mathbf{Q}(t)$.

The solution to (26) provides a refined covariance matrix that captures both the deterministic and stochastic aspects of uncertainty propagation over time.

The reachable set $\mathcal{S}_j^t$ as shown in Fig. 3 at time t is defined through the uncertainty ellipsoid:

$$\mathcal{S}_j^t = \{\mathbf{x} : (\mathbf{x} - \bar{\mathbf{x}}_j(t))^\top \mathbf{\Sigma}_j^{-1}(t)(\mathbf{x} - \bar{\mathbf{x}}_j(t)) \leq \gamma\}, \quad (27)$$

where $\bar{\mathbf{x}}_j(t)$ denotes the nominal predicted state and γ defines the confidence level.

To maintain prediction reliability with computational efficiency, we introduce an adaptive confidence measure:

$$\alpha_j(t) = \exp(-\lambda \text{tr}(\mathbf{\Sigma}_j(t))), \quad (28)$$

where λ is a positive scaling parameter and $\text{tr}(\mathbf{\Sigma}_j(t))$ denotes the trace of the covariance matrix. This measure governs the adaptive prediction horizon through:

$$N_p(k) = \min\{N_{p,\max}, \max\{N_{p,\min}, \lceil \frac{N_{p,\max}}{\alpha_j(k)} \rceil\}\}, \quad (29)$$

where $N_{p,\max}$ and $N_{p,\min}$ represent the maximum and minimum allowable prediction horizons respectively, and k denotes the current time step. The resulting prediction framework provides probabilistic state estimates for surrounding vehicles while maintaining computational tractability through adaptive horizon adjustment. These predictions directly inform the subsequent MPC optimization by defining probabilistic constraints on vehicle interactions and enabling risk-aware decision making. The complete derivation of the discrete-time prediction framework is presented in Appendix B.

C. Game-Theoretic MPC with Uncertainty-Aware Prediction

The prediction mechanism integrates with the game-theoretic decision making through the adaptive horizon mechanism. Building upon the vehicle dynamics in (19) and linearized error dynamics in (21), an integrated optimization problem is formulated that incorporates both prediction uncertainties and game-theoretic objectives.

The predicted states from the adaptive framework inform the Stackelberg game solver through a constrained weighted sum optimization:

$$\begin{aligned} \tilde{\mathbf{u}}_{\text{SV}}^*(k) = \arg\max_{\tilde{\mathbf{u}}_{\text{SV}}} \min_{\tilde{\mathbf{y}} \in \mathcal{Y}} & \sum_{i=k}^{k+N_p(k)} \alpha_j(i) P_{\text{SV}}(\tilde{\mathbf{u}}_{\text{SV}}(i), \tilde{\mathbf{y}}(i)) \\ \text{s.t. } & (21), (18), d_j(i) \geq d_{\text{safe}}, \forall j \in \{\text{PV}, \text{RV}, \text{IV}\}, \\ & i = k, \ldots, k + N_p(k), \end{aligned} \quad (30)$$

where $N_p(k)$ is the adaptive prediction horizon at time step k, $\alpha_j(i)$ represents the prediction confidence defined by the covariance growth, and P_{SV} denotes the payoff function incorporating safety, efficiency, and comfort objectives as defined in (5). The constraints ensure satisfaction of linearized vehicle dynamics, physical limitations on velocity, steering and acceleration, and safe distances d_j from other vehicles.

The adaptive integration mechanism operates on multiple levels. First, the prediction horizon $N_p(k)$ adjusts dynamically based on the uncertainty bounds defined by $\mathbf{\Sigma}_j(t)$, ensuring reliable predictions within computational constraints. Second, the confidence measure $\alpha_j(i)$ weights the strategic decisions according to prediction reliability, with higher weights assigned to near-term predictions where uncertainty is lower.

To establish robust stability guarantees for the prediction framework, we analyze the bounds on the linearized error dynamics in (21). The evolution of prediction errors is characterized by:

$$\|\tilde{\mathbf{x}}(t)\| \leq \gamma_1 \|\tilde{\mathbf{x}}(0)\| + \gamma_2 \sup_{0 \leq \tau \leq t} \|\tilde{\mathbf{y}}(\tau)\| \text{ s.t. } \gamma_1, \gamma_2 > 0, \quad (31)$$

where γ_1 bounds the growth of initial state errors and γ_2 characterizes the system's sensitivity to environmental uncertainties. These bounds are derived from the Jacobian matrices J_1 and J_3, respectively, with γ_1 determined by the maximum eigenvalue of J_1 and γ_2 by the induced norm of J_3. The stability certificates ensure that prediction errors remain bounded even as uncertainties accumulate over the prediction horizon, enabling reliable trajectory planning under both normal and emergency scenarios.

Despite its adaptive capabilities, the game-theoretic framework faces fundamental limitations when uncertainty becomes excessive or spatial constraints become severe. In such critical scenarios, we transition to a hybrid potential field method (Section V) that provides more efficient reactive capabilities while maintaining essential safety guarantees.

D. Computational Limitations in Emergency Scenarios

While the Stackelberg framework provides strategic advantages, its computational complexity grows exponentially with uncertainty and spatial constraints. The equilibrium computation requires solving:

$$\mathcal{C}(\tilde{\mathbf{u}}_{\text{SV}}^*) = O(|\mathcal{U}_{\text{SV}}| \cdot \prod_{i \in \{\text{PV}, \text{RV}, \text{IV}\}} |\mathcal{U}_i^*|), \quad (32)$$

where $|\mathcal{U}_i^*|$ represents the cardinality of vehicle i's best-response strategy set. Under high uncertainty, these sets expand significantly as:

$$|\mathcal{U}_i^*(t)| \propto \exp(\lambda_c \cdot \text{tr}(\mathbf{\Sigma}_i(t))), \quad (33)$$

where $\lambda_c > 0$ is the complexity growth rate parameter, and $\mathbf{\Sigma}_i(t)$ is the prediction covariance matrix defined in (24). This exponential growth makes real-time computation infeasible when $\text{tr}(\mathbf{\Sigma}_i(t))$ exceeds critical thresholds. Furthermore, when spatial constraints tighten ($d_{\text{avail}} \to d_{\text{safe}}$), the feasible strategy space becomes fragmented, causing convergence issues in the iterative equilibrium solver. These fundamental limitations motivate our hybrid approach, where potential fields provide computationally efficient reactive control when strategic planning becomes intractable.

V. Hybrid Potential Field Approach

The game-theoretic and potential field approaches serve complementary roles in our framework, each suited to different operational regimes defined by uncertainty and urgency.

Game theory enables strategic multi-agent coordination over extended horizons with complexity $O(n^3)$ for n agents, but becomes computationally intractable and spatially infeasible in emergency scenarios where prediction errors amplify and maneuvering gaps shrink. In contrast, potential fields offer instantaneous responses with linear complexity $O(n)$, providing robust reactivity and guaranteed efficiency. Our hybrid approach leverages these complementary strengths through adaptive mode switching: under normal conditions the system pursues globally optimal game-theoretic planning, while in emergencies it transitions to potential field control, prioritizing safety and responsiveness over long-horizon optimality.

A. Mode Switching Mechanism

Building upon the emergency characterization in Section II, our system employs a dynamic switching mechanism based on continuous risk assessment. When environmental conditions exceed safe thresholds for game-theoretic reasoning, the system transitions to reactive potential field control:

$$\text{Mode}(t) = \begin{cases} \text{Game-theoretic}, & \Gamma(t) < \Gamma_{\text{thr}}(t) \\ \text{Potential field}, & \Gamma(t) \geq \Gamma_{\text{thr}}(t) \end{cases}. \tag{34}$$

The composite risk function $\Gamma(t) = \sum_i w_i \gamma_i(t)$ aggregates multiple normalized indicators: prediction uncertainty $1/\alpha_j(t)$, potential field ratio, velocity differential, and spatial feasibility $S(t) = d_{\text{avail}}(t)/d_{\text{req}}(t)$. Notably, the prediction uncertainty indicator $1/\alpha_j(t)$ implicitly captures deviations from the rational behavior patterns assumed in the game-theoretic model, as human drivers may exhibit bounded rationality due to cognitive limitations and varying risk preferences. This allows the switching mechanism to naturally transition to potential field control when surrounding vehicles' behaviors deviate significantly from game-theoretic predictions. Here, $d_{\text{avail}}(t)$ represents the actual available gap between vehicles, $d_{\text{req}}(t)$ represents the minimum required gap based on reaction time, braking distance, and dynamic safety margins. The threshold $\Gamma_{\text{thr}}(t)$ adapts based on contextual factors such as distance to the exit point, becoming more sensitive as the vehicle approaches critical decision points.

B. Uncertainty-Aware Risk Field

Central to our approach is incorporating prediction uncertainty directly into the risk assessment. For each surrounding vehicle, we construct a probabilistic risk field that combines static and dynamic risk factors:

$$R_i(x, y, t) = [R_i^{\text{pos}}(x, y) + R_i^{\text{vel}}(x, y)] \cdot \Psi_i(x, y, t). \tag{35}$$

The position-based component R_i^{pos} models collision risk using Gaussian distributions in the vehicle-centered frame, while the velocity-dependent component R_i^{vel} accounts for relative motion as shown in Fig. 4. The uncertainty modulation factor Ψ_i amplifies risk in proportion to prediction uncertainty:

$$\Psi_i(x, y, t) = 1 + \lambda_\Psi \exp\left(-\frac{\|(x, y) - (\bar{x}_i, \bar{y}_i)\|^2}{2\lambda_d \cdot \text{tr}(\mathbf{\Sigma}_i(t))}\right), \tag{36}$$

where $\mathbf{\Sigma}_i(t)$ is the prediction covariance matrix in (24), λ_Ψ is a scaling coefficient for uncertainty influence, $(\bar{x}_i, \bar{y}_i)$ represents the predicted mean position of vehicle i, and λ_d controls the spatial extent of uncertainty effects. This integration ensures that areas with higher prediction uncertainty generate proportionally higher risk values.

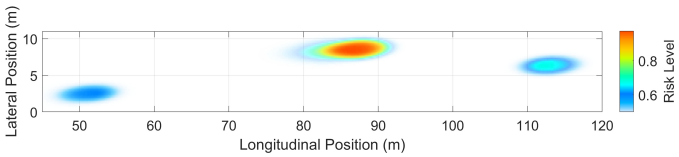

Fig. 4: Illustration of the dynamic risk field.

A key feature of our design is that all spatial parameters scale with uncertainty. For example, the standard deviations in the risk field expand as prediction confidence decreases:

$$\sigma_x(t) = \sigma_{x,0} + \gamma_x \sqrt{\mathbf{\Sigma}_i^{xx}(t)}, \sigma_y(t) = \sigma_{y,0} + \gamma_y \sqrt{\mathbf{\Sigma}_i^{yy}(t)}, \tag{37}$$

where $\sigma_{x,0}$ and $\sigma_{y,0}$ are baseline spatial parameters representing nominal risk field size, γ_x and γ_y are scaling factors that determine how strongly uncertainty affects risk distribution, and $\mathbf{\Sigma}_i^{xx}(t)$ and $\mathbf{\Sigma}_i^{yy}(t)$ are the position variance components extracted from the covariance matrix. This scaling creates larger risk regions around vehicles with uncertain predicted trajectories, naturally promoting more conservative behavior when prediction reliability diminishes.

C. Potential Field Formation and Decision Logic

The total potential guiding the autonomous vehicle combines attractive forces toward the lane center and repulsive forces from surrounding vehicles:

$$U_{\text{total}}(x, y, t) = \sum_{i=1}^{4} k_i U_i(x, y, t), \tag{38}$$

where $U_1 = U_{\text{lane}}$, $U_2 = U_{\text{PV}}$, $U_3 = U_{\text{S2}}$, and $U_4 = U_{\text{unc}}$ denote the attractive lane potential, repulsion from the preceding vehicle, surrounding vehicle influence, and uncertainty-weighted potential field, respectively. U_{lane} enforces lane-keeping through a quadratic potential, U_{PV} and U_{S2} represent repulsive potentials from preceding and surrounding vehicles based on their risk fields, and U_{unc} adds explicit uncertainty-based repulsion. The coefficient $k_4 = k_{4,0}(1-\alpha_j(t))$ increases the influence of uncertainty as prediction confidence decreases.

Lane-changing decisions emerge naturally from the potential field structure. A lane change is triggered when the repulsive potentials overwhelm the lane-keeping attraction:

$$U_{\text{PV}} + U_{\text{S2}} + U_{\text{unc}} \geq \beta(t) \cdot U_{\text{lane}}, \tag{39}$$

where $\beta(t) = \beta_0 \exp(-\lambda d_{\text{PV}}) \cdot (1 + \mu \cdot \text{tr}(\mathbf{\Sigma}_{\text{PV}}(t)))$ adapts to both proximity and uncertainty. Here, β_0 is a baseline threshold coefficient, λ is a distance-sensitivity parameter that modulates the effect of distance to the PV d_{PV}, and μ is an uncertainty-weighting factor that scales the influence of prediction uncertainty represented by the trace of the covariance matrix $\mathbf{\Sigma}_{\text{PV}}(t)$. This formulation enables more aggressive evasive maneuvers when necessary while maintaining safety margins to prediction uncertainty as shown in Fig. 5.

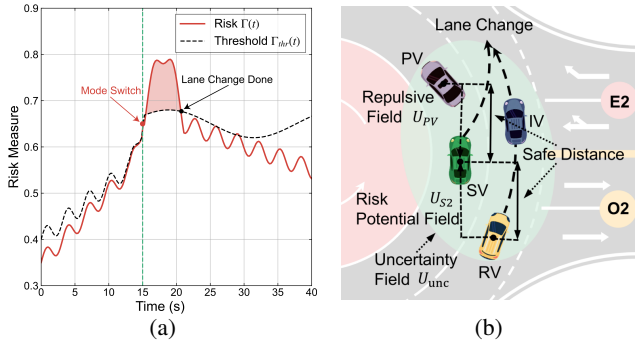

(a) (b)

Fig. 5: Mode switching: (a) Risk measure vs. threshold showing switch point and lane change; (b) Components of the hybrid potential field during lane changing.

D. Trajectory Generation

Once a lane change is triggered, smooth trajectories are generated using quintic polynomials that ensure continuity in position, velocity, and acceleration:

$$f(t) = \sum_{k=0}^{5} a_k t^k, \quad t_{\text{start}} < t < t_{\text{end}}, \tag{40}$$

where $f(t)$ represents the position trajectory along either the x or y axis, a_k are the polynomial coefficients determined by boundary conditions (initial and final position, velocity, and acceleration), and t_{start} and t_{end} define the time interval for the lane change maneuver.

The polynomial coefficients a_k are determined through constrained optimization:

$$\min_{a_k} \int_{t_{\text{start}}}^{t_{\text{end}}} (\dddot{f}(t))^2 dt, \text{s.t. (1), (16), and (18)} \tag{41}$$

ensuring the generated trajectory respects vehicle dynamics limits including lateral acceleration $a_y \leq \mu g$ and steering constraints inherited from the vehicle model in (16).

A key innovation is uncertainty-aware goal adjustment, where the terminal waypoint shifts based on prediction uncertainty:

$$[x_f, y_f] = [x_{f,0}, y_{f,0}] + \lambda_d \cdot \sqrt{\text{tr}(\mathbf{\Sigma}_{\text{PV}}(t))} \cdot \mathbf{d}_{\text{norm}}, \tag{42}$$

where $[x_{f,0}, y_{f,0}]$ is the nominal final position, and $\mathbf{d}_{\text{norm}}$ is the normalized direction vector away from potential collision points. This adjustment creates larger safety margins when prediction uncertainty is high.

The potential field mechanism complements the game-theoretic layer, providing reactive capabilities for emergency situations while preserving the uncertainty-awareness established in our prediction framework.

VI. Simulation Results

The proposed method is evaluated against the baseline Nash equilibrium approach [20] using Matlab 2023b. The baseline implements a simultaneous non-cooperative game where all vehicles make decisions concurrently without hierarchy, contrasting with our Stackelberg approach where the SV acts as a committed leader influencing others' responses.

TABLE I: Key Parameters Used in the Simulation.

Component	Parameter	Value
Vehicle Dynamics	Maximum velocity ($v_{\max}$)	15 m/s
	Maximum acceleration ($a_{\max}$)	5 m/s^2
	Maximum deceleration ($a_{\min}$)	-5 m/s^2
	Safe distance (d_{safe})	5 m
Stackelberg Game	Safety weight (C_{s}^{SV})	0.6
	Efficiency weight (C_{e}^{SV})	0.3
	Comfort weight (C_{c}^{SV})	0.1
	Attention allocation ($\varepsilon_1^{\text{SV}}$)	1.5
	Attention allocation ($\varepsilon_2^{\text{SV}}$)	1.2
Uncertainty Prediction	Initial position variance ($\sigma_{x,0}^2, \sigma_{y,0}^2$)	(0.1, 0.1) m^2
	Growth rate ($\epsilon_x^2, \epsilon_y^2$)	(0.05, 0.05) m^2/s
	Heading variance ($\sigma_{\phi,0}^2$)	0.01 rad^2
	Prediction horizon ($N_{p,\max}$)	5 s
Hybrid Potential Field	Repulsive weight (k_2)	0.7
	Attractive weight (k_1)	0.3
	Risk amplitude (A_s)	1.0
	Lane-change threshold (β_0)	0.85
MPC Controller	Sampling time (T_s)	0.1 s
	Control horizon (N_c)	10 steps
	Constraint satisfaction tolerance(ς)	10^{-4}

Both methods use identical profit functions but differ in their solution concept: simultaneous mutual best responses (Nash) versus sequential leader-follower optimization (Stackelberg). Simulation parameters are summarized in Table I, with weights empirically tuned to balance safety and efficiency. Both methods use identical initial conditions, convergence criteria ($\varsigma = 10^{-4}$, 50 iterations), and an MPC framework (2.0 s horizon, 0.1 s step), differing only in decision strategy: Stackelberg-based optimization versus simultaneous best response. Performance is assessed through arrival rate, collision rate, travel time, and key trajectory statistics across two cases—one under normal conditions, and another involving emergency overtaking maneuvers.

A. Case 1: Normal Situations

TABLE II:
Algorithm Performance Comparison in Outlet 4.

Methods	Average Arrive Rate (%)	Average Collision Rate (%)	Average Simulation Time (s)
Ours	$\mathbf{94.72 \pm 3.16}$	$\mathbf{0.94 \pm 1.09}$	$\mathbf{41.7 \pm 7.5}$
Nash	72.43 ± 5.27	11.27 ± 4.15	58.4 ± 6.1

A typical roundabout scenario is selected to represent normal situations. Fig. 6 illustrates the comparative performance analysis between our Stackelberg approach and the Nash equilibrium method for outlet O4. Fig. 6(a) and Fig. 6(b) show the trajectory patterns through the roundabout, where both methods achieve collision-free navigation. Our approach demonstrates more consistent spacing between vehicles and smoother trajectory curves, particularly evident in the extended circular section required for reaching the fourth exit.

The acceleration distributions shown in the top row of Fig. 6(c) and Fig. 6(d) highlight the enhanced stability of our approach. Under the Stackelberg method, acceleration distributions are more tightly concentrated near zero, with RV showing a particularly sharp peak, indicating smoother

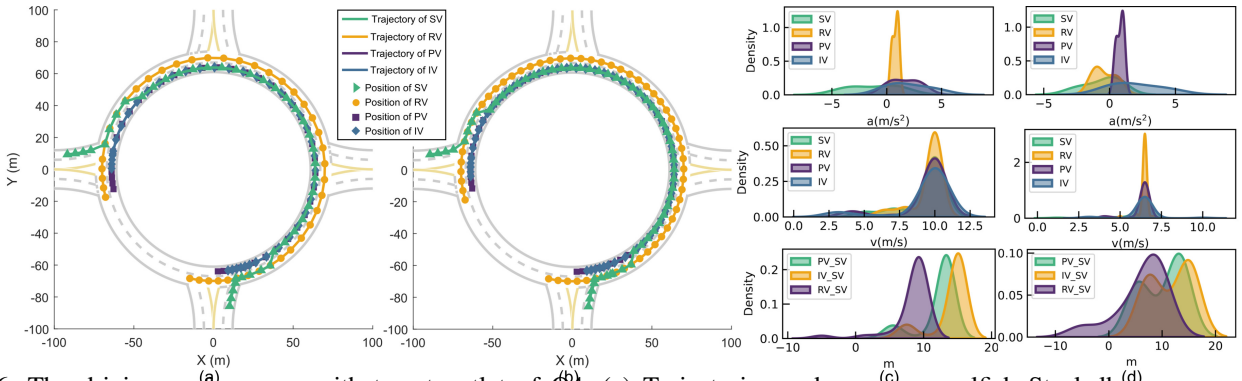

Fig. 6: The driving performance with target outlet of O4. (a) Trajectories under our non-selfish Stackelberg approach; (b) Trajectories under baseline Nash equilibrium method; (c) Distribution of accelerations, velocities, and relative distances under our approach; (d) Distribution of accelerations, velocities, and relative distances under baseline Nash equilibrium method.

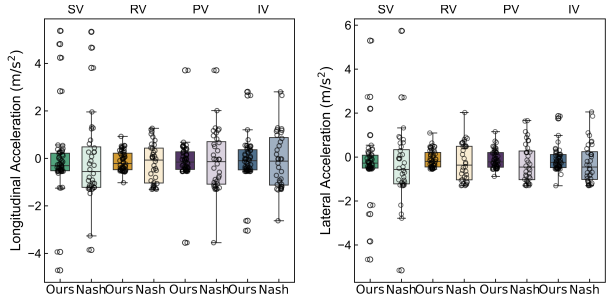

Fig. 7: Box plots of accelerations: (a) Longitudinal accelerations; and (b) Lateral accelerations.

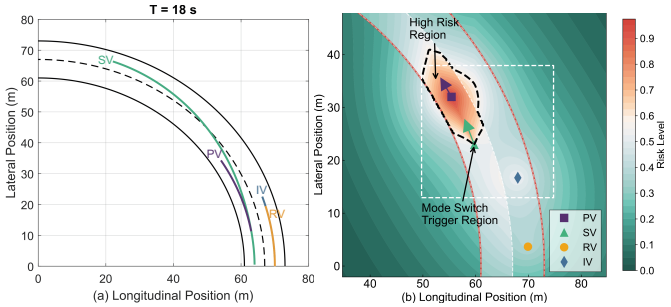

Fig. 8: Emergency scenario: (a) Spatial trajectories with SV lane change at t=18 s; (b) Risk heatmap showing high-risk area, mode switch trigger zone, and vehicle positions.

driving behavior. In contrast, the Nash method exhibits broader acceleration distributions with multiple peaks, suggesting more frequent and abrupt speed adjustments.

The velocity profiles presented in the middle row of Fig. 6(c) and Fig. 6(d) reveal superior speed management in our approach. The Stackelberg method maintains more uniform velocity distributions around 7.5 m/s, with well-synchronized patterns between vehicles. The Nash equilibrium method, however, shows more dispersed velocity distributions extending beyond 10 m/s, indicating less coordinated speed control and potentially more aggressive driving behavior.

The relative distance analysis in the bottom row of Fig. 6(c) and Fig. 6(d) demonstrates the improved spatial coordination of our approach. Under the Stackelberg method, relative distances between vehicle pairs show compact distributions centered around 10 m, while the Nash method exhibits wider spreads up to 20 m. This indicates that our approach achieves more efficient space utilization and better maintains safe distance throughout the roundabout maneuver. Note that although the spatial trajectories in Fig. 6(a) and Fig. 6(b) appear similar, their temporal dynamics differ markedly. The Stackelberg approach yields smoother velocities and steadier spacing, while the Nash method shows frequent speed changes and larger variations. These distinctions are evident in the distribution plots Fig. 6(c) and Fig. 6(d), where "Density" denotes normalized PDFs with different scales reflecting the concentration of accelerations, velocities, and distances.

Fig. 7 presents box plots comparing acceleration characteristics for both methods in the O4 scenario, highlighting distinct performance differences. In the longitudinal dimension (Fig. 7(a)), our Stackelberg approach shows improved stability, with SV exhibiting a more concentrated distribution around zero and fewer outliers compared to the Nash method's wider range of -4 – $5\,\mathrm{m/s^2}$. For lateral acceleration (Fig. 7(b)), our method achieves smaller interquartile ranges and fewer extreme outliers, particularly for SV and RV. In contrast, the Nash method shows larger variations and extreme lateral movements, with SV reaching up to $6\,\mathrm{m/s^2}$. These results demonstrate that our approach ensures more stable and comfortable vehicle control throughout the roundabout maneuver.

Table II demonstrates the superior performance of our Stackelberg approach in the complex O4 scenario. Our method achieves a significantly higher arrival rate $94.7 \pm 3.16\%$ vs $72.43 \pm 5.27\%$ and substantially lower collision rate $0.94 \pm 1.09\%$ vs $11.27 \pm 4.15\%$ compared to the Nash method. Furthermore, our approach completes the navigation more efficiently with an average simulation time of 41.7 ± 7.5 s, notably faster than Nash's $(58.4 \pm 6.1\,\mathrm{s})$, validating its effectiveness in complex roundabout scenarios.

B. *Case 2: Emergency Mode Switching*

To evaluate our system's adaptive capabilities, we designed a scenario where the autonomous vehicle transitions from

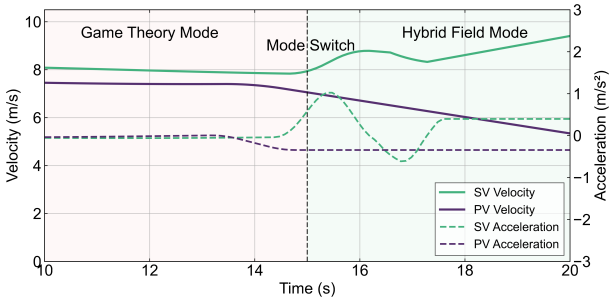

Fig. 9: Velocity and acceleration profiles during mode switch at t=15 s, showing the transition from game-theoretic to hybrid field control due to PV deceleration.

game-theoretic to hybrid potential field control when confronted with an emergency situation. The spatial trajectory analysis in Fig. 8(a) shows the SV successfully executing a lane change from inner to outer lane by $t = 18$ s, adapting to the complex geometric constraints of the roundabout's north-eastern quadrant. The hybrid potential field method effectively generates appropriate repulsive forces from the PV while maintaining safe distances from other vehicles.

Fig. 8(b) illustrates the risk heatmap and mode switching mechanism during the emergency scenario. The heatmap visualizes risk levels across spatial positions, with the highest risk region (red) concentrated around the PV. The SV is positioned at the edge of the mode switch trigger region (white dashed rectangle), which activates the transition from game-theoretic to hybrid potential field control. The black dashed contour demarcates the high-risk region where immediate reactive control becomes necessary, while red contour lines indicate risk threshold boundaries. This visualization demonstrates how the risk level increases as distance to the PV decreases, and how our system adaptively adjusts its control strategy based on dynamically assessed risk levels. The spatial distribution of vehicles—PV (purple square), SV (green triangle), RV (orange circle), and IV (blue diamond)—shows their relative positions during this critical transition phase.

Fig. 9 shows the velocity and acceleration profiles during the mode switching process. At $t = 15$ s, the system transitions from game-theoretic control to the hybrid potential field method in response to the PV's sudden deceleration. Before switching, both SV and PV maintain stable velocities (approximately 8 m/s and 7.8 m/s) with acceleration fluctuations below ± 0.5 m/s^2. When the PV begins decelerating to -0.5 m/s^2 at $t = 15$ s, the system's risk assessment triggers the mode switch. The hybrid field controller responds with a characteristic acceleration pattern, then increasing to 1.5 m/s^2 to execute the lane change. This adaptive response enables the SV to maintain a relatively consistent velocity despite the disturbance, stabilizing at approximately 9 m/s by $t = 19$ s while keeping acceleration changes within comfortable limits (± 1 m/s^2) throughout the transition.

C. Computational Performance Analysis

We evaluated our framework on an Intel Core i5-12600KF CPU (3.70 GHz) with 64 GB RAM. As detailed in Table III,

TABLE III:
COMPUTATIONAL PERFORMANCE ANALYSIS.

Algorithm Component	Computation Time (ms)		
	Mean	Std	Max
State Prediction	8.4	1.2	11.7
Stackelberg Game Solver	28.7	3.2	36.5
Hybrid Potential Field	12.3	1.5	15.8
MPC Trajectory Generation	15.9	2.1	21.3
Total (Normal Mode)	53.0	4.3	63.2
Total (Emergency Mode)	36.6	2.8	42.5

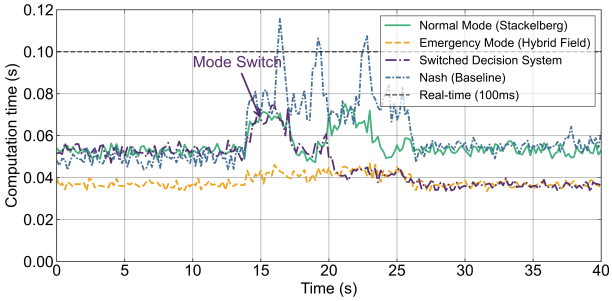

Fig. 10: Computational analysis showing the efficiency of the Stackelberg approach and the higher efficiency of the hybrid potential field method in emergencies.

the Stackelberg game solver requires 28.7 ± 3.2 ms per decision cycle, while the hybrid potential field method needs only 12.3 ± 1.5 ms, demonstrating its suitability for emergency scenarios requiring rapid responses. The complete decision cycle averages 53.0 ms in normal mode and 36.6 ms in emergency mode, with maximum observed times of 63.2 ms and 42.5 ms respectively. Both operational modes comfortably satisfy our 100 ms real-time constraint.

Fig. 10 further illustrates the computational efficiency of our approach across different traffic scenarios. During normal operation, the Stackelberg-based decision system maintains stable computation times around 0.055 s, less than the Nash baseline. When the SV encounter interaction conflicts ($\sim$ 15 s), the Nash equilibrium approach exhibits significant computational spikes exceeding 0.1 s, surpassing the real-time threshold. In contrast, our switched decision system intelligently transitions to the emergency mode, leveraging the more efficient hybrid potential field method throughout the conflict. This adaptive switching mechanism ensures that our system remains responsive and reliable even in complex, safety-critical traffic situations. The computationally intensive game-theoretic approach is reserved for non-emergency scenarios where strategic decision-making is not time-critical.

VII. CONCLUSION

This paper presents an uncertainty-aware framework for autonomous driving in roundabouts that effectively balances safety, efficiency, and cooperation under both normal and emergency conditions. The proposed system combines probabilistic prediction with game theory to enable strategic planning under uncertainty during normal operation, while seamlessly transitioning to a hybrid potential field approach when emergency maneuvers are required. Extensive simula-

tions demonstrate that our method significantly outperforms baseline approaches in terms of navigation success rate and collision avoidance. Future work will focus on incorporating learning-based mechanisms to enhance prediction accuracy. The framework will also be extended to handle more complex multi-vehicle scenarios with heterogeneous agent behaviors, comprehensive analysis of roundabout entry performance, and system-level evaluation of traffic efficiency improvements across different penetration rates of AVs.

APPENDIX

This appendix provides derivations of the vehicle prediction with uncertainty. We first present the continuous-time system linearization, followed by the discrete-time prediction formulation with explicit uncertainty propagation.

A. System Linearization and Uncertainty Characterization

Starting from the nonlinear vehicle dynamics in (16) with process uncertainty, and the compact form in (19)

For linearization around a reference trajectory $(\mathbf{x}_r, \mathbf{u}_r, \mathbf{y}_r)$, first-order Taylor expansion of (20) is

$$\begin{aligned}\dot{\mathbf{x}} &= f(\mathbf{x}_r, \mathbf{u}_r, \mathbf{y}_r) + \frac{\partial f}{\partial \mathbf{x}}(\mathbf{x} - \mathbf{x}_r) \\ &+ \frac{\partial f}{\partial \mathbf{u}}(\mathbf{u} - \mathbf{u}_r) + \frac{\partial f}{\partial \mathbf{y}}(\mathbf{y} - \mathbf{y}_r) + \mathbf{w}(t).\end{aligned} \tag{43}$$

The Jacobian matrices derived through partial differentiation are:

$$J_1 = \left.\frac{\partial f}{\partial \mathbf{x}}\right|_{\substack{\mathbf{x}=\mathbf{x}_r \\ \mathbf{u}=\mathbf{u}_r \\ \mathbf{y}=\mathbf{y}_r}} = \begin{bmatrix} 0 & 0 & -v_r \sin(\phi_r) \\ 0 & 0 & v_r \cos(\phi_r) \\ 0 & 0 & 0 \end{bmatrix}, \tag{44}$$

$$J_2 = \left.\frac{\partial f}{\partial \mathbf{u}}\right|_{\substack{\mathbf{x}=\mathbf{x}_r \\ \mathbf{u}=\mathbf{u}_r \\ \mathbf{y}=\mathbf{y}_r}} = \begin{bmatrix} \cos(\phi_r) & 0 \\ \sin(\phi_r) & 0 \\ \frac{\tan(\delta_r)}{L} & \frac{v_r}{L\cos^2(\phi_r)} \end{bmatrix}, \tag{45}$$

$$J_3 = \left.\frac{\partial f}{\partial \mathbf{y}}\right|_{\substack{\mathbf{x}=\mathbf{x}_r \\ \mathbf{u}=\mathbf{u}_r \\ \mathbf{y}=\mathbf{y}_r}} = \begin{bmatrix} \frac{\partial f_1}{\partial \mathbf{x}_{\text{PV}}} & \frac{\partial f_1}{\partial \mathbf{x}_{\text{RV}}} & \frac{\partial f_1}{\partial \mathbf{x}_{\text{IV}}} \\ \frac{\partial f_2}{\partial \mathbf{x}_{\text{PV}}} & \frac{\partial f_2}{\partial \mathbf{x}_{\text{RV}}} & \frac{\partial f_2}{\partial \mathbf{x}_{\text{IV}}} \\ \frac{\partial f_3}{\partial \mathbf{x}_{\text{PV}}} & \frac{\partial f_3}{\partial \mathbf{x}_{\text{RV}}} & \frac{\partial f_3}{\partial \mathbf{x}_{\text{IV}}} \end{bmatrix}. \tag{46}$$

Defining error states $\tilde{\mathbf{x}} = \mathbf{x} - \mathbf{x}_r$, $\tilde{\mathbf{u}} = \mathbf{u} - \mathbf{u}_r$, and $\tilde{\mathbf{y}} = \mathbf{y} - \mathbf{y}_r$, we can get the (21).

B. Discrete-Time System and Prediction Framework

Building on the continuous-time formulations (21) and (26) from the main text, we now derive their discrete-time counterparts for use in MPC. The continuous-time system (21) is discretized with sampling time T. Using an Euler approximation for simplicity, we have:

$$\tilde{\mathbf{x}}(k+1) = A\tilde{\mathbf{x}}(k) + B\tilde{\mathbf{u}}(k) + C\tilde{\mathbf{y}}(k) + \mathbf{w}_d(k), \tag{47}$$

where the discrete-time system matrices are derived:

$$A = I + T \cdot J_1, \quad B = T \cdot J_2, \quad C = T \cdot J_3. \tag{48}$$

When transitioning from the continuous-time formulation to the discrete-time setting for numerical implementation, the continuous-time process noise covariance $\mathbf{Q}(t)$ is converted into a corresponding discrete-time covariance $\mathbf{Q}_d$. Specifically, $\mathbf{Q}_d = \int_0^T e^{J_1\tau}\mathbf{Q}e^{J_1^\top\tau}\mathrm{d}\tau$ is obtained by integrating the continuous-time covariance over the interval $[0, T]$. This ensures that the discrete-time system accurately reflects the accumulated process noise over one sampling interval T.

To incorporate states and time-varying uncertainties in prediction, we define an augmented state vector including both error states and uncertainty terms. Using the notation from the main text and $\mathbf{\Sigma}_j(t)$ in (24), we have:

$$\xi(k) = [\tilde{\mathbf{x}}(k) \quad \tilde{\mathbf{u}}(k-1) \quad \tilde{\mathbf{y}}(k-1) \quad \mathbf{\Sigma}_j(k)]^\top, \tag{49}$$

where $\mathbf{\Sigma}_j(k)$ is the discrete-time counterpart of the continuous uncertainty covariance $\mathbf{\Sigma}_j(t)$.

The augmented state evolution follows from substituting the discrete-time dynamics and uncertainty propagation:

$$\begin{aligned}\xi(k+1) = &\begin{bmatrix} A\tilde{\mathbf{x}}(k) + B\tilde{\mathbf{u}}(k-1) + C\tilde{\mathbf{y}}(k-1) \\ \tilde{\mathbf{u}}(k-1) \\ \tilde{\mathbf{y}}(k-1) \\ A\mathbf{\Sigma}_j(k)A^\top + \mathbf{Q}_d \end{bmatrix} \\ &+ \begin{bmatrix} B\Delta\tilde{\mathbf{u}}(k) + C\Delta\tilde{\mathbf{y}}(k) \\ \Delta\tilde{\mathbf{u}}(k) \\ \Delta\tilde{\mathbf{y}}(k) \\ 0 \end{bmatrix},\end{aligned} \tag{50}$$

where $\Delta\tilde{\mathbf{u}}(k) = \tilde{\mathbf{u}}(k) - \tilde{\mathbf{u}}(k-1)$ and $\Delta\tilde{\mathbf{y}}(k) = \tilde{\mathbf{y}}(k) - \tilde{\mathbf{y}}(k-1)$.

This can be written compactly as:

$$\xi(k+1) = \bar{A}\xi(k) + \bar{B}\Delta\tilde{\mathbf{w}}(k) \tag{51}$$

with augmented system matrices:

$$\bar{A} = \begin{bmatrix} A & B & C & 0 \\ 0 & I & 0 & 0 \\ 0 & 0 & I & 0 \\ 0 & 0 & 0 & \mathcal{A} \end{bmatrix}, \quad \bar{B} = \begin{bmatrix} B & C \\ I & 0 \\ 0 & I \\ 0 & 0 \end{bmatrix}, \tag{52}$$

where the uncertainty propagation operator $\mathcal{A}$ is defined as:

$$\mathcal{A} = APA^\top + \mathbf{Q}_d. \tag{53}$$

We also define a measurement equation that incorporates uncertainty:

$$\eta(k) = \bar{H}\xi(k) = \begin{bmatrix} H & 0 & 0 & H_\Sigma \end{bmatrix} \xi(k), \tag{54}$$

where H maps states to measurements and H_Σ extracts uncertainty information.

For a prediction horizon N_p and control horizon N_c ($N_p \geq N_c$), the predicted state evolution is:

$$\begin{aligned}\xi(k+j) &= \bar{A}^j\xi(k) + \sum_{i=0}^{j-1} \bar{A}^{j-1-i}\bar{B}\Delta\tilde{\mathbf{w}}(k+i), \\ \mathbf{\Sigma}_j(k+j) &= \mathcal{A}^j\mathbf{\Sigma}_j(k) + \sum_{i=0}^{j-1} \mathcal{A}^{j-1-i}\mathbf{Q}_d.\end{aligned} \tag{55}$$

The complete output prediction incorporating uncertainties is given by:

$$Y = \Phi\xi(k) + \Gamma W + \Psi\mathbf{W} + \Lambda\mathbf{\Sigma}, \tag{56}$$

where:

$$\Phi = \begin{bmatrix} \bar{H}\bar{A} \\ \bar{H}\bar{A}^2 \\ \vdots \\ \bar{H}\bar{A}^{N_p} \end{bmatrix}, \quad \Lambda = \begin{bmatrix} H_\Sigma \\ H_\Sigma \mathcal{A} \\ \vdots \\ H_\Sigma \mathcal{A}^{N_p} \end{bmatrix},$$

$$\Gamma = \begin{bmatrix} \bar{H}\bar{B} & 0 & \cdots & 0 \\ \bar{H}\bar{A}\bar{B} & \bar{H}\bar{B} & \cdots & 0 \\ \vdots & \vdots & \ddots & \vdots \\ \bar{H}\bar{A}^{N_p-1}\bar{B} & \bar{H}\bar{A}^{N_p-2}\bar{B} & \cdots & \bar{H}\bar{B} \end{bmatrix}, \tag{57}$$

$$\Psi = \begin{bmatrix} H & 0 & \cdots & 0 \\ H\bar{A} & H & \cdots & 0 \\ \vdots & \vdots & \ddots & \vdots \\ H\bar{A}^{N_p-1} & H\bar{A}^{N_p-2} & \cdots & H \end{bmatrix}.$$

The probabilistic prediction bounds are characterized by:

$$\Pr\{\|\eta(k+j|k) - \bar{\eta}(k+j|k)\| \leq \epsilon_j\} \geq 1 - \alpha_j, \tag{58}$$

where ϵ_j represents the error bound and α_j defines the confidence level at prediction step j.

REFERENCES

[1] S. Hou, C. Wang, and J. Gao, "Reinforced stable matching for crowd-sourced delivery systems under stochastic driver acceptance behavior," *Transp. Res. Part C: Emerg. Technol.*, vol. 170, p. 104916, 2025.

[2] Y. Yuan, S. Li, L. Yang, and Z. Gao, "Nonlinear model predictive control to automatic train regulation of metro system: An exact solution for embedded applications," *Automatica*, vol. 162, p. 111533, 2024.

[3] Y. Shi, Z. Gu, X. Yang, Y. Li, and Z. Chu, "An adaptive route guidance model considering the effect of traffic signals based on deep reinforcement learning," *IEEE Intell. Transp. Syst. Mag.*, vol. 16, no. 3, pp. 21–34, 2024.

[4] W. Wu, Y. Zhu, and R. Liu, "Dynamic scheduling of flexible bus services with hybrid requests and fairness: Heuristics-guided multi-agent reinforcement learning with imitation learning," *Transp. Res. Part B: Methodol.*, vol. 190, p. 103069, 2024.

[5] K. Xu, C. G. Cassandras, and W. Xiao, "Decentralized time and energy-optimal control of connected and automated vehicles in a roundabout with safety and comfort guarantees," *IEEE Trans. Intell. Transp. Syst.*, vol. 24, no. 1, pp. 657–672, 2023.

[6] M. Lv, Y. Li, H. Liang, B. Sun, C. Yang, and W. Gui, "A spatial–temporal variational graph attention autoencoder using interactive information for fault detection in complex industrial processes," *IEEE Trans. Neural Netw. Learn. Syst.*, vol. 35, no. 3, pp. 3062–3076, 2024.

[7] M. Cao, K. Cao, S. Yuan, T.-M. Nguyen, and L. Xie, "Neptune: Nonentangling trajectory planning for multiple tethered unmanned vehicles," *IEEE Trans. Robot.*, vol. 39, no. 4, pp. 2786–2804, 2023.

[8] D. J. Kim, Y. W. Jeong, and C. C. Chung, "Lateral vehicle trajectory planning using a model predictive control scheme for an automated perpendicular parking system," *IEEE Trans. Ind. Electron.*, vol. 70, no. 2, pp. 1820–1829, 2023.

[9] J. Hu, Y. Zhang, and S. Rakheja, "Adaptive lane change trajectory planning scheme for autonomous vehicles under various road frictions and vehicle speeds," *IEEE Trans. Intell. Veh.*, vol. 8, no. 2, pp. 1252–1265, 2023.

[10] Z. Hong, Q. Lin, and B. Hu, "Knowledge distillation-based edge-decision hierarchies for interactive behavior-aware planning in autonomous driving system," *IEEE Trans. Intell. Transp. Syst.*, vol. 25, no. 9, pp. 11040–11057, 2024.

[11] K. Yang *et al.*, "Towards robust decision-making for autonomous driving on highway," *IEEE Trans. Veh. Technol.*, vol. 72, no. 9, pp. 11 251–11 263, 2023.

[12] L. Bai, F. Zheng, K. Hou, X. Liu, L. Lu, and C. Liu, "Longitudinal control of automated vehicles: A novel approach by integrating deep reinforcement learning with intelligent driver model," *IEEE Trans. Veh. Technol.*, vol. 73, no. 8, pp. 11 014–11 028, 2024.

[13] X. Chen, Y. Sun, T. Zhang, X. Wang, S. Xiong, and K. Cao, "An anytime trajectory optimizer for accurately parking an autonomous vehicle in tiny spaces," *IEEE Trans. Veh. Technol.*, pp. 1–12, 2025.

[14] J. Yu, P.-A. Laharotte, Y. Han, W. Ma, and L. Leclercq, "Perimeter control with heterogeneous metering rates for cordon signals: A physics-regularized multi-agent reinforcement learning approach," *Transp. Res. Part C: Emerg. Technol.*, vol. 171, p. 104944, 2025.

[15] Z. Lin, J. Lan, C. Anagnostopoulos, Z. Tian, and D. Flynn, "Safety-critical multi-agent mcts for mixed traffic coordination at unsignalized intersections," *IEEE Trans. Intell. Transp. Syst.*, pp. 1–15, 2025.

[16] X. Shi and X. Li, "Empirical study on car-following characteristics of commercial automated vehicles with different headway settings," *Transp. Res. Part C: Emerg. Technol.*, vol. 128, p. 103134, 2021.

[17] J. Zhu, S. Easa, and K. Gao, "Merging control strategies of connected and autonomous vehicles at freeway on-ramps: A comprehensive review," *J. Intell. Connected Vehicles*, vol. 5, no. 2, pp. 99–111, 2022.

[18] M. Yuan, J. Shan, and H. Schofield, "Scalable game-theoretic decision-making for self-driving cars at unsignalized intersections," *IEEE Trans. Ind. Electron.*, vol. 71, no. 6, pp. 5920–5930, 2024.

[19] D. Li, J. Zhang, and G. Liu, "Autonomous driving decision algorithm for complex multi-vehicle interactions: An efficient approach based on global sorting and local gaming," *IEEE Trans. Intell. Transp. Syst.*, vol. 25, no. 7, pp. 6927–6937, 2024.

[20] P. H. et al., "Driving conflict resolution of autonomous vehicles at unsignalized intersections: A differential game approach," *IEEE/ASME Trans. Mechatron.*, vol. 27, no. 6, pp. 5136–5146, 2022.

[21] R. Chandra and D. Manocha, "Gameplan: Game-theoretic multi-agent planning with human drivers at intersections, roundabouts, and merging," *IEEE Robot. Autom. Lett.*, vol. 7, no. 2, pp. 2676–2683, 2022.

[22] P. Hang, C. Huang, Z. Hu, Y. Xing, and C. Lv, "Decision making of connected automated vehicles at an unsignalized roundabout considering personalized driving behaviours," *IEEE Trans. Veh. Technol.*, vol. 70, no. 5, pp. 4051–4064, 2021.

[23] G. Zhang, J. Xie, B. Peng, H. Zhang, and D. Song, "Power allocation strategy of multi-static radar network tracking maneuvering jammer based on stackelberg game," *IEEE Trans. Veh. Technol.*, pp. 1–10, 2025.

[24] Z. Lin, Z. Tian, J. Lan, Q. Zhang, Z. Ye, H. Zhuang, and X. Zhao, "A conflicts-free, speed-lossless kan-based reinforcement learning decision system for interactive driving in roundabouts," *IEEE Trans. Intell. Transp. Syst.*, vol. 25, pp. 1–14, 2025.

[25] Z. Tian *et al.*, "Efficient and balanced exploration-driven decision making for autonomous racing using local information," *IEEE Trans. on Intell. Veh.*, vol. 10, no. 3, pp. 1732–1748, 2025.

[26] X. Liu, M. Yu, C. Yang, L. Zhou, H. Wang, and H. Zhou, "Value distribution ddpg with dual-prioritized experience replay for coordinated control of coal-fired power generation systems," *IEEE Trans. Ind. Inf.*, vol. 20, no. 6, pp. 8181–8194, June 2024.

[27] J. Xi, F. Zhu, P. Ye, Y. Lv, G. Xiong, and F.-Y. Wang, "Auxiliary network enhanced hierarchical graph reinforcement learning for vehicle repositioning," *IEEE Trans. Intell. Transp. Syst.*, vol. 25, no. 9, pp. 11 563–11 575, Sept. 2024.

[28] X. Ma and X. He, "Providing real-time en-route suggestions to cavs for congestion mitigation: A two-way deep reinforcement learning approach," *Transp. Res. Part B: Methodol.*, vol. 189, p. 103014, 2024.

[29] J. Wang and L. Sun, "Robust dynamic bus control: A distributional multi-agent reinforcement learning approach," *IEEE Trans. Intell. Transp. Syst.*, vol. 24, no. 4, pp. 4075–4088, 2023.

[30] S. Mak, L. Xu, T. Pearce, M. Ostroumov, and A. Brintrup, "Fair collaborative vehicle routing: A deep multi-agent reinforcement learning approach," *Transp. Res. Part C: Emerg. Technol.*, vol. 157, p. 104376, 2023.

[31] Y. Zhu, Z. Wang, Y. Zhu, C. Chen, and D. Zhao, "Discretizing continuous action space with unimodal probability distributions for on-policy reinforcement learning," *IEEE Trans. Neural Netw. Learn. Syst.*, pp. 1–13, 2024.

[32] P. Cai *et al.*, "Dq-gat: Towards safe and efficient autonomous driving with deep q-learning and graph attention networks," *IEEE Trans. Intell. Transp. Syst.*, vol. 23, no. 11, pp. 21 102–21 112, 2022.

[33] B. Peng *et al.*, "Communication scheduling by deep reinforcement learning for remote traffic state estimation with bayesian inference," *IEEE Trans. Veh. Technol.*, vol. 71, no. 4, pp. 4287–4300, 2022.

[34] T. Xia, H. Chen, J. Yang, and Z. Guo, "Geometric field model of driver's perceived risk for safe and human-like trajectory planning," *Transp. Res. Part C: Emerg. Technol.*, vol. 159, p. 104470, 2024.

[35] Y. Gao, D. Li, Z. Sui, and Y. Tian, "Trajectory planning and tracking control of autonomous vehicles based on improved artificial potential field," *IEEE Trans. Veh. Technol.*, vol. 73, no. 9, pp. 12468–12483, 2024.

[36] R. Szczepanski, "Safe artificial potential field: Novel local path planning algorithm maintaining safe distance from obstacles," *IEEE Robot. Autom. Lett.*, vol. 8, no. 8, pp. 4823–4830, 2023.
[37] L. Zhang, Y. Dong, H. Farah, and B. van Arem, "Social-aware planning and control for automated vehicles based on driving risk field and model predictive contouring control: Driving through roundabouts as a case study," in *2023 IEEE Int. Conf. Syst., Man, Cybern. (SMC)*, 2023, pp. 3297–3304.
[38] L. Xue, G.-P. Liu, and W. Hu, "All-in-one framework for design, simulation, and practical implementation of distributed multiagent control systems," *IEEE Trans. Syst., Man, Cybern.: Syst.*, vol. 54, no. 7, pp. 4331–4344, 2024.
[39] W. Zhong, X. Huang, Y. Wu, R. Yu, and J. Kang, "Decentralized energy management for wireless power transfer assisted platoon autonomous driving: A leader-to-follower approach," *IEEE Trans. Green Commun. Netw.*, vol. 6, no. 4, pp. 2073–2083, 2022.
[40] P. Zhou, X. Sun, and T. Chai, "Enhanced nmpc for stochastic dynamic systems driven by control error compensation with entropy optimization," *IEEE Trans. Control Syst. Technol.*, vol. 31, no. 5, pp. 2217–2230, 2023.
[41] J. Zhang, S.-C. Chai, B.-H. Zhang, and G.-P. Liu, "Distributed model-free sliding-mode predictive control of discrete-time second-order nonlinear multiagent systems with delays," *IEEE Trans. Cybern.*, vol. 52, no. 11, pp. 12 403–12 413, 2022.
[42] H. Qi, C. Chen, X. Hu, and J. Zhang, "Online inference of lane changing events for connected and automated vehicle applications with analytical logistic diffusion stochastic differential equation," *Transp. Res. Part C Emerg. Technol.*, vol. 144, p. 103874, 2022.
[43] G. H. Lee, D.-H. Kim, J. M. Pak, and C. K. Ahn, "Vehicle sideslip angle estimation using finite memory estimation and dynamics/kinematics model fusion based on neural networks," *IEEE Trans. Intell. Transp. Syst.*, vol. 26, no. 2, pp. 2157–2168, 2025.
[44] J. Wurts, J. L. Stein, and T. Ersal, "Design for real-time nonlinear model predictive control with application to collision imminent steering," *IEEE Trans. Control Syst. Technol.*, vol. 30, no. 6, pp. 2450–2465, 2022.

Zhihao Lin received an M.S. degree from the College of Electronic Science & Engineering, Jilin University, Jilin, China. He is currently pursuing a Ph.D. degree with the College of Science and Engineering, University of Glasgow, Glasgow, U.K. His main research interests focus on multi-sensor fusion SLAM systems, reinforcement learning, and hybrid control of vehicle platoons.

Zhen Tian received his bachelor degree in electronic and electrical engineering from the University of Strathclyde, Glasgow, U.K. in 2020. He is currently pursuing the Ph.D. degree with the College of Science and Engineering, University of Glasgow, Glasgow, U.K. His main research interests include Interactive vehicle decision system and autonomous racing decision systems.

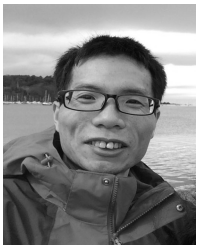

Jianglin Lan received a Ph.D. degree from the University of Hull in 2017. He has been a Leverhulme Early Career Fellow and Lecturer at the University of Glasgow since 2022. He was a Visiting Professor at the Robotics Institute, Carnegie Mellon University, in 2023. From 2017 to 2022, he held postdoc positions at Imperial College London, Loughborough University, and University of Sheffield. His research interests include safe AI, control theory, and autonomy.

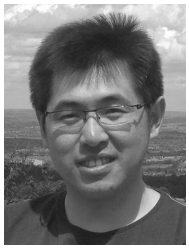

Dezong Zhao received the Ph.D. degree in Control Engineering from Tsinghua University, Beijing, China, in 2010. He is a Professor of Autonomous Systems with the University of Glasgow and a Turing Fellow with The Alan Turing Institute. He was awarded a a Royal Society of Engineering / Leverhulme Trust Research Fellow in 2025, a Royal Society-Newton Advanced Fellow in 2020 and an EPSRC Innovation Fellow in 2018.

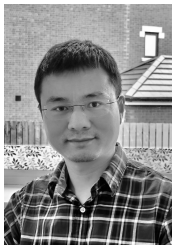

Chongfeng Wei received his Ph.D. degree in mechanical engineering from the University of Birmingham in 2015. He is now an Associate Professor (University Senior Lecturer) at University of Glasgow, UK. His current research interests include decision-making and control of intelligent vehicles, human-centric autonomous driving, cooperative automation, and dynamics and control of mechanical systems. He is also serving as an Associate Editor of IEEE TITS, IEEE TIV, IEEE TVT, and Frontier on Robotics and AI.